Available online at www.sciencedirect.com
ScienceDirect
Earth and Planetary Science Letters 258 (2007) 593–604
EPSL
www.elsevier.com/locate/epsl

Timing of the Early Triassic carbon cycle perturbations inferred from new U–Pb ages and ammonoid biochronozones

Thomas Galfetti [a,*], Hugo Bucher [a], Maria Ovtcharova [b], Urs Schaltegger [b], Arnaud Brayard [a,c], Thomas Brühwiler [a], Nicolas Goudemand [a], Helmut Weissert [d], Peter A. Hochuli [a], Fabrice Cordey [c], Kuang Guodun [e]

[a] *Paläontologisches Institut der Universität Zürich, Karl Schmid-Strasse 4, 8006 Zürich, Switzerland*
[b] *Department of Mineralogy, University of Geneva, rue des Maraîchers 13, CH-1205 Geneva, Switzerland*
[c] *UMR 5125 PEPS CNRS, Université Lyon I, Campus de la Doua, 69622 Villeurbanne Cedex, France*
[d] *Department of Earth Science, ETH, Sonneggstrasse 5, 8006 Zürich, Switzerland*
[e] *Guangxi Bureau of Geology and Mineral Resources, Jiangzheng Road 1, 530023 Nanning, China*

Received 13 October 2006; received in revised form 3 April 2007; accepted 13 April 2007
Available online 20 April 2007
Editor: H. Elderfield

Abstract

Based on analyses of single, thermally annealed and chemically abraded zircons, a new high-precision U–Pb age of 251.22 ± 0.20 Ma is established for a volcanic ash layer within the "*Kashmirites densistriatus* beds" of early Smithian age (Early Triassic) from the Luolou Formation (northwestern Guangxi, South China). This new date, together with recalculated uncertainties of previous U–Pb ages from the same section [M. Ovtcharova, H. Bucher, U. Schaltegger, T. Galfetti, A. Brayard, J. Guex. New Early to Middle Triassic U–Pb ages from South China: calibration with ammonoid biochronozones and implications for the timing of the Triassic biotic recovery. Earth Planet. Sci. Lett. 243 (2006) 463–475.] allows constraining the time framework of the Early Triassic and leads to an estimated duration of (i) ca. 0.7 ± 0.6 My for the Smithian and (ii) a maximal duration of ca. 1.4 ± 0.4 My for the Griesbachian–Dienerian time interval. The new U–Pb age considerably reduces the absolute age gap comprised between the Permian–Triassic boundary and the Spathian (late Early Triassic).

The new age framework provides the basis for the calibration of a new carbonate carbon isotope and ammonoid records of the Early Triassic Luolou Fm., which in turn are of high significance for global correlations and for carbon cycle modeling. This calibration indicates that the most significant and fastest Early Triassic carbon isotope perturbations occur between the earliest Smithian and the early Spathian, thus spanning a time interval of about 1 My. Whatever caused these carbon cycle shifts of high intensity and short duration, there is evidence for connections between these fluctuations, the pulsate recovery of ammonoids and conodonts as well as climate changes.

Keywords: carbon isotope; U–Pb age; time scale; ammonoid; Early Triassic; South China

* Corresponding author. Fax: +41 44 634 49 23.
E-mail addresses: galfetti@pim.uzh.ch (T. Galfetti), hugo.FR.bucher@pim.uzh.ch (H. Bucher), maria.ovtcharova@terre.unige.ch (M. Ovtcharova), urs.schaltegger@terre.unige.ch (U. Schaltegger), arnaud.brayard@univ-lyon1.fr (A. Brayard), bruehwiler@pim.uzh.ch (T. Brühwiler), goudemand@pim.uzh.ch (N. Goudemand), helmut.weissert@erdw.ethz.ch (H. Weissert), peter.hochuli@erdw.ethz.ch (P.A. Hochuli), Fabrice.Cordey@univ-lyon1.fr (F. Cordey).

0012-821X/$ - see front matter © 2007 Elsevier B.V. All rights reserved.
doi:10.1016/j.epsl.2007.04.023

1. Introduction

Large carbon cycle fluctuations are known to occur in the aftermath of the end-Permian mass extinction (e.g. [1–6]). Crucial for carbon cycle modeling and for the interpretation of carbon isotope signals is a precise time framework based on the calibration of high-resolution ammonoid zones with high-precision radiometric ages. Up till now radiometric ages were available only for the Spathian (late Early Triassic) [7]. A minimal duration of 4.5±0.6 My for the Early Triassic has been established [7] and subsequently an estimate of ca. 5 My has been proposed [8]. Both estimates, which rely on the age of the Permian–Triassic boundary of 252.6±0.2 Ma [9], reveal a duration of the Spathian of at least half of the entire Early Triassic. The radio-isotopic age gap comprised between the Permian–Triassic boundary and the Spathian has hampered the establishment of a precise time frame of the initial phase of the Early Triassic biotic recovery and the calibration of the major fluctuations of the C-isotope record. Thus, the new early Smithian U–Pb age presented here provides crucial information for a new age model.

The new early Smithian U–Pb date, together with recalculated uncertainties of Early and Middle Triassic ages [7] and the refined calibration of ammonoid zonation, provides for the first time a precise timing of the globally recognized carbon cycle perturbations (e.g. [10,11,2–4,6,12]) during Early Triassic times.

2. Geological setting and paleontological age control

Carbon isotope and volcanic ash layer samples were collected from the Early Triassic outer platform series of the Nanpanjiang Basin (South China Block) (see Lehrmann et al. [13] for a description of this basin). The studied Early Triassic series at Jinya/Waili (northwestern Guangxi; Fig. 1) belongs to the Luolou Formation and consists of a mixed carbonate–siliciclastic, ammonoid- and conodont-rich sedimentary succession (Fig. 2). At Jinya/Waili, the base of the Luolou Fm. starts with a ~7-m-thick unit composed of calcimicrobial limestones. This unit apparently conformably overlies the Late Permian Wujiaping Fm. The presence of foraminifers such as *Earlandia* sp., *Rectocornuspira kalhori*, *Spirorbis phlyctaena*, *Cornuspira mahajeri* as well as the ostracod *Liuzhinia antalyaensis*[1] [14,15], 2 and 7 m above the base of the calcimicrobial limestone suggest a Griesbachian age for this unit. The calcimicrobial limestone is overlain by a ~40-m-thick mixed series of thin-bedded, dark, laminated, suboxic limestones alternating with dark, organic-rich shales. As suggested by poorly preserved ammonoids (?*Ophiceras* sp.), the lowermost part of this unit could still be of (late) Griesbachian age. The next younger ammonoid fauna is an assemblage (*Ambites*, *Vishnuites* and *Meekophiceras*) that correlates with the North American Candidus Zone of early Dienerian age. The rest of the Dienerian fossil record is poor. Early Smithian faunas occur some 10 m higher up ("*Hedenstroemia hedenstroemi* beds" and "*Kashmirites densistriatus* beds"). A prominent, cliff-forming, ~3 m thick, bioturbated limestone of middle Smithian age (i.e. "*Flemingites rursiradiatus* beds") occurs ca. 15 m above the base of the mixed series. Black, laminated and organic-rich anoxic shales enclosing early diagenetic limestone concretions invariably underlie the "*F. rursiradiatus* beds". A second interval of similar lithology consistently occurs at the very end of the Smithian (i.e. "*Anasibirites multiformis* beds"). The next overlying ~40-m-thick unit is almost exclusively composed of grey, nodular, and highly bioturbated limestones. As indicated by ammonoids, the deposition of this massive carbonate succession spans almost the entire Spathian, from the earliest "Tirolitid n. gen. A beds" (Ovtcharova et al. [7] and Bucher et al., ongoing work) to the Haugi Zone. Only the "*Courtilloticeras stevensi* beds" of the latest Spathian [16,17] have not been documented. The transition from the Luolou Fm. to the overlying Baifeng Fm. is marked by a conspicuous ~15-m-thick unit composed of nodular siliceous limestones termed "Transition beds". A newly documented radiolarian assemblage occurring ~1 m above the base of these beds comprises the taxa *Eptingium* sp., *Pantanellium* sp., *Plafkerium* sp., and *Pseudostylosphaera* sp., along with 6-spine spumellarians (gen. et sp. indet.) [18]. This association correlates with the TR2A or TR2B assemblage zones of early Anisian age [19], and thus demonstrates the absence of a significant gap within this unit. The "Transition beds" are overlain by a very thick series (>1000 m) of thickening and coarsening upward siliciclastic turbidites (Baifeng Fm.). A few thin carbonate layers are still intercalated within the basal, predominantly shaly part of this prograding turbiditic series.

In addition to the two previously dated volcanic ash layers, which invariably occur in the lower and upper Spathian [7], we report here a new 2-cm-thick, fine-grained volcanic ash bed (CHIN-40) occurring within the "*K. densistriatus* beds" of early Smithian age (Fig. 2).

[1] In the eastern Sichuan Province, Kershaw et al. [14] found the ostracod *Liuzhinia antalyaensis* associated with the earliest Triassic conodont marker *Hindeodus parvus* (Kozur and Pjatakova).

Fig. 1. Location map of the Jinya/Waili area and other sites mentioned in the text.

3. U–Pb zircon geochronology

As discussed in many papers (e.g. [20,9,21]) high-precision ID-TIMS (Isotope Dilution Thermal Ionization Mass Spectrometry), U–Pb analyses on single-zircon crystals are commonly applied for dating volcanic ash layers. We assume that the zircon crystallization age closely approximates that of the volcanic eruption and ash layer deposition. Zircon is the preferred mineral for dating sedimentary sequences because of its lowest diffusion coefficients for Pb and U [22] and highest resistance against post-crystallization system disturbance. Nevertheless, complications in getting precise and accurate zircon ages may arise mainly by following effects: (1) post-crystallization lead loss and; (2) incorporation of old cores acting as nuclei during crystallization, or more generally, of foreign lead with a radiogenic composition indicative for a pre-ash depositional age. To minimize the probability of inheritance and reliable dating, mainly single zircon grains are selected for analyses after preliminary microscopic inspection in transmitted light. Following the chemical abrasion (CA) technique [23], all the grains were subjected to high temperature annealing and HF leaching procedure, which recently proved to be most efficient in eliminating of the discordance caused by Pb loss [9]. Theoretically, successful application of CA technique ensures "close system" behavior of the residual zircon and thus single grain analyses yielding a tight concordant cluster of U–Pb ages with precisions better than 0.1%. Additional complication arises from the small sample size, the relatively low concentration of U and young age, resulting in low amounts of radiogenic Pb for analysis. This requires low analytical blanks and good control of the blank isotopic composition.

During the last few years, determination of analytical uncertainties and error propagation became an important issue for intercalibrating geochronologic data between different laboratories. Many publications highlight the differences between random (or internal) and systematic (external) errors emphasizing that systematic errors should be propagated when comparing dates from different laboratories and the uranium decay uncertainties should be incorporated when comparing data from different geochronologic methods [24–26]. This requires not only incorporation of systematic errors but also agreement on the algorithms of error propagation and statistical analysis of U–Pb and $^{40}Ar/^{39}Ar$ data, especially for the purposes of geologic time scale calibration. In most recent studies data reduction and age calculation are done using PbMacDat (Coleman, unpublished), where error propagation is given by equations of Ludwig [27]. Another program for age calculation and error propagation is ROMAGE (Davis, unpublished). This latter program was used to data reduction of zircon U–Pb ages from Early and Middle Triassic volcanic ash layers from South China [7], using measured $^{207}Pb/^{205}Pb$ ratios for the determination of radiogenic lead concentration. In order to make this previous data comparable with other recent publications concerning similar time-scale problems (e.g. [28,8]), we recalculated our data using the PbMacDat program and the algorithms of Ludwig [27], using measured $^{206}Pb/^{205}Pb$ ratios for radiogenic lead concentration calculation. The uncertainties of the tracer and blank lead isotopic composition and of mass fractionation correction are propagated to the final uncertainties of isotopic ratios and ages. Uncertainties are therefore strictly comparable to the "external uncertainties" of Lehrmann et al. [8], Schoene and Bowring [25] and Schoene et al. [26]. We therefore refer to the Early and Middle Triassic age values reported in Ovtcharova et al. [7] with the following recalculated uncertainties: sample CHIN-10 ("*Tirolites*/*Columbites* beds"): 250.55 ± 0.40 Ma; sample CHIN-23 (*N. haugi* Zone): 248.12 ± 0.28 Ma; sample CHIN-29 (*A. hyatti* Zone): 246.83 ± 0.31 Ma and sample CHIN-34 (*B. shoshonensis* Zone): 244.60 ± 0.36 Ma. U–Pb ages with recalculated uncertainties are marked with an asterisk (*) in Figs. 2 and 4.

The analytical procedures used for U–Pb dating used in this study are identical to those described in Ovtcharova et al. [7]. Data reduction and age calculation have been done using the algorithms of Ludwig [27], while generation of concordia plots and calculation of

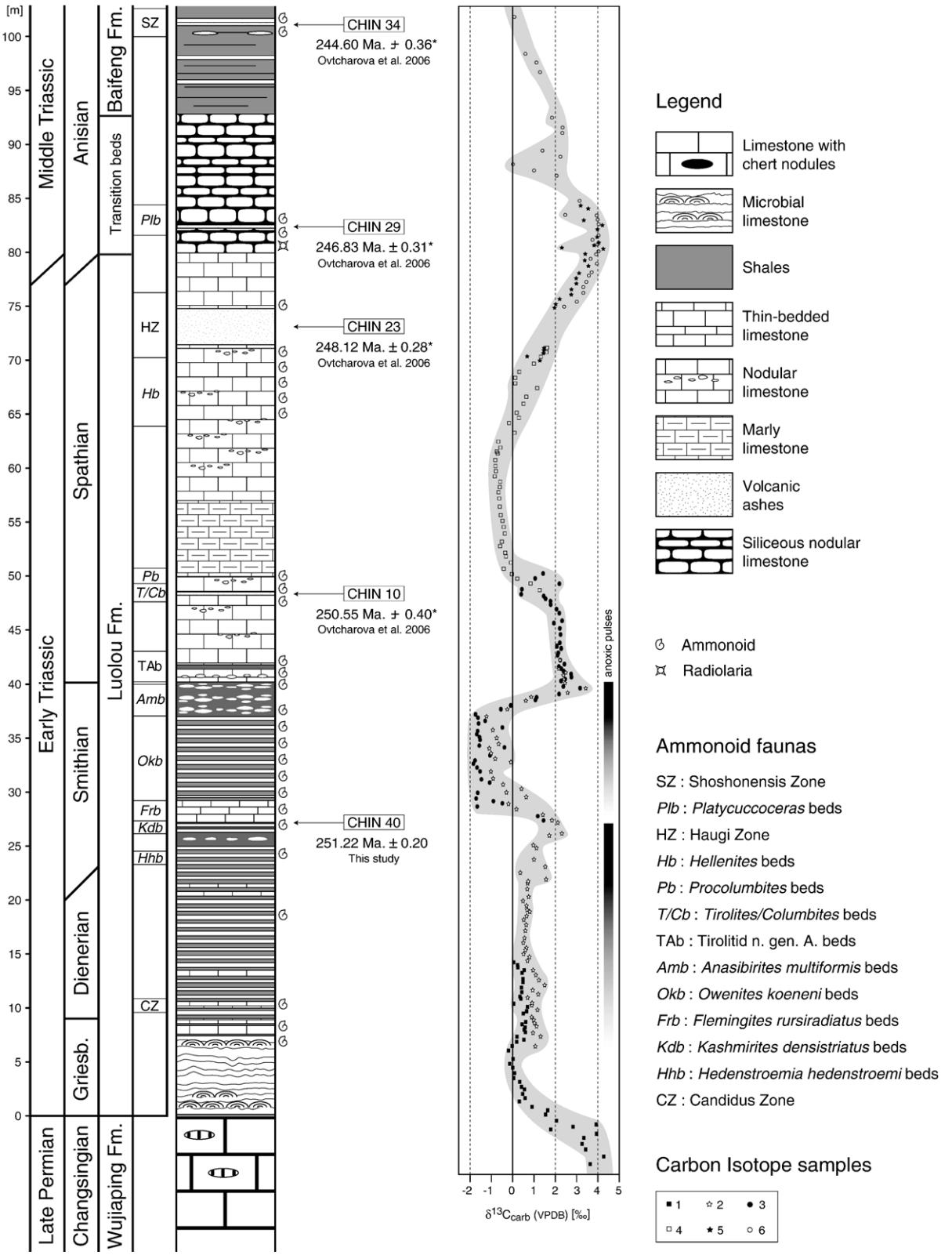
[m]
Middle Triassic
Early Triassic
Late Permian
Anisian
Spathian
Smithian
Dienerian
Griesb.
Changsingian
Baifeng Fm.
Transition beds
Luolou Fm.
Wujiaping Fm.
SZ
Plb
HZ
Hb
Pb
T/Cb
TAb
Amb
Okb
Frb
Kdb
Hhb
CZ
CHIN 34
244.60 Ma. ± 0.36*
Ovtcharova et al. 2006
CHIN 29
246.83 Ma. ± 0.31*
Ovtcharova et al. 2006
CHIN 23
248.12 Ma. ± 0.28*
Ovtcharova et al. 2006
CHIN 10
250.55 Ma. ± 0.40*
Ovtcharova et al. 2006
CHIN 40
251.22 Ma. ± 0.20
This study
anoxic pulses
δ13Ccarb (VPDB) [‰]
Legend
Limestone with chert nodules
Microbial limestone
Shales
Thin-bedded limestone
Nodular limestone
Marly limestone
Volcanic ashes
Siliceous nodular limestone
Ammonoid
Radiolaria
Ammonoid faunas
SZ : Shoshonensis Zone
Plb : Platycuccoceras beds
HZ : Haugi Zone
Hb : Hellenites beds
Pb : Procolumbites beds
T/Cb : Tirolites/Columbites beds
TAb : Tirolitid n. gen. A. beds
Amb : Anasibirites multiformis beds
Okb : Owenites koeneni beds
Frb : Flemingites rursiradiatus beds
Kdb : Kashmirites densistriatus beds
Hhb : Hedenstroemia hedenstroemi beds
CZ : Candidus Zone
Carbon Isotope samples
1 2 3
4 5 6

weighted mean have been done with the program Isoplot/Ex v.3 of Ludwig [29].

3.1. Results: sample CHIN-40

Zircons from sample CHIN-40 are short to long prismatic (up to 200 μm in their longest dimensions), often cracked, rich in apatite and fluid inclusions. Six single long prismatic crystals were analyzed from this sample (analytical data are given in Table 1). All the analyses (Fig. 3) are concordant within analytical error and define a weighted mean $^{206}Pb/^{238}U$ age of 251.22±0.20 Ma (MSWD=0.4), which we consider the best estimate for the age of these zircons and inferentially the volcanic ash bed within the early Smithian "*K. densistriatus* beds" fauna.

4. Calibration of ammonoid biochronozones with U–Pb ages and implications

All new and previously published U–Pb ages with recalculated uncertainties and the ammonoid succession available from the Luolou Fm. (updated from Ovtcharova et al. [7]) are summarized in Fig. 4.

The implicit assumption of equal zone duration as used in the recent Triassic time scale [30] has been demonstrated to be largely erroneous [31,7]. During times of extreme fluctuations of taxonomic diversity, such as during the Early Triassic [32], the disparity between equal zone duration and effective duration significantly aggravates [31]. The obviously uneven duration of zones stresses the need for independent calibration of the Early Triassic ammonoid zones by means of radio-isotopic ages.

Until a more thorough knowledge of Early Triassic ammonoid faunas is achieved, we prefer the term "beds" rather than "Zone" for age-diagnostic associations, which have not already been formally defined as zones. This is meant to avoid unnecessary profusion of zonal names until a paleogeographically comprehensive data set of Early Triassic ammonoid data will be processed with the Unitary Associations method [33].

Following the definitions for the mid-/high-latitude records [34,35], the base of the Smithian is assumed here at the base of the "*H. hedenstroemi* beds". Another option for the base of the Smithian (i.e. the base of the Olenekian) is currently being discussed within the frame of the Subcommission of Triassic Stratigraphy. According to this proposal, the "*F. rursiradiatus* beds" and their worldwide correlatives would define the base of the Smithian. Until a formal agreement on a new definition of the base of the Olenekian is reached, we use the mid/high latitudinal definition of the Smithian [34,35].

Considering a 250.55 Ma±0.40 Ma age for the early Spathian (i.e. "*Tirolites*/*Columbites* beds" – CHIN-10; [7]) and the new U–Pb age associated with the early Smithian "*K. densistriatus* beds" fauna (i.e. CHIN-40: 251.22±0.20 Ma, this study), an estimated duration of ca. 0.7±0.6 My can be inferred for the Smithian substage. This new age constraint emphasizes the extremely high rate of the ammonoid diversification during mid-Smithian times ("*F. rursiradiatus* beds" and "*Owenites koeneni* beds").

Additionally, taking into account the Permian–Triassic boundary age of 252.6±0.2 Ma [9] and the early Smithian "*K. densistriatus* beds" age of 251.22±0.20 Ma, a maximal duration of ca. 1.4±0.4 My can be inferred for the Griesbachian–Dienerian interval. As already pointed out by Ovtcharova et al. [7], the 251.4±0.3 Ma age of Bowring et al. [36] for the Permian–Triassic boundary leads to an unrealistic estimate of the duration of the Early Triassic stages. Moreover, this previous age estimate of the Permian–Triassic boundary conflicts with our new early Smithian age in that it would imply an extremely short duration of ca. 200±500 ky (!) for the Griesbachian–Dienerian interval.

5. Early Triassic carbonate carbon isotope record

5.1. Samples and analytical technique

High-resolution sampling (10–40 cm) was carried out throughout the entire Early Triassic sedimentary succession. Samples were cautiously cleaned, cut in thin slabs and selectively drilled with a diamond-tipped drill to produce a fine powder.

Carbonate carbon and oxygen isotopes measurements ($\delta^{13}C_{carb}$ and $\delta^{18}O_{carb}$) were performed at the Institute of Mineralogy and Geochemistry of Lausanne

Fig. 2. Jinya/Waili composite section of the Luolou and Baifeng Fm. with: (i) the stratigraphic position of the new (CHIN-40; GPS position: N24°35′23.5″/E106°52′49.6″) and previously analyzed ash beds [7] (CHIN-10/23/29/34). The recalculated analytical uncertainties of previously published U–Pb ages [7] are marked with an asterisk (*) (see Section 3 for further details); (ii) composite carbonate carbon isotope data and (iii) anoxic trends (darker shading denotes greater intensity of anoxia). Compiled sections: (1) Laren PTB Section (GPS position: N24°36′32.6″, E106°52′28.9″; (2) Waili Fall Section (GPS position: N24°35′07.1″, E106°52′59.9″; (3) Laren Road-cut Section (GPS position: N24°36′23.6″, E106°52′37.9″); (4) Waili Panorama Section (GPS position: N24°35′19.8″, E106°52′59.6″); (5) Wan Tuo Section (GPS position: N24°35′30.9″, E106°51′45.9″); (6) Waili Fall Transition beds Section (GPS position: N24°35′01.7″, E106°53′03.5″).

Table 1
U–Pb isotopic data of analyzed zircons

Sample no.	Weight (mg)	Concentration			Th/U [a]	Isotopic ratios							Correlation coefficient	Ages (Ma)		
		U (ppm)	Pb (ppm)	Pb com. pg		206/204 [b]	207/206 [c,d]	Error (%) [e]	207/235 [c]	Error	206/238 [c/d]	Error 2σ (%)		$^{206}Pb/^{238}U$	$^{207}Pb/^{235}U$	$^{207}Pb/^{206}Pb$
CHIN-40																
1	0.0012	324	13.60	0.91	0.53	197	0.051700	1.19	0.283200	1.27	0.039720	0.18	0.50	251.13	253.19	272.38
2	0.0010	131	5.84	1.23	0.64	72	0.052850	3.80	0.290040	4.00	0.039800	0.29	0.71	251.62	258.59	322.32
3	0.0010	196	8.56	1.58	0.51	80	0.051870	3.27	0.284470	3.43	0.039770	0.26	0.64	251.42	254.19	279.85
4	0.0007	185	7.80	0.76	0.55	1405	0.051370	0.24	0.281380	0.31	0.039730	0.20	0.63	251.15	251.75	257.41
5	0.0007	329	13.90	0.62	0.58	2657	0.051410	0.14	0.281580	0.23	0.039710	0.18	0.79	251.14	251.91	259.11
6	0.0014	654	27.44	0.75	0.54	1993	0.051210	0.15	0.280600	0.25	0.039740	0.18	0.81	251.20	251.13	250.48

[a] Calculated based on radiogenic $^{208}Pb/^{206}Pb$ ratios, assuming concordance.
[b] Corrected for fractionation and spike.
[c] Corrected for fractionation, spike and blank (all common lead was assumed to be procedural blank).
[d] Corrected for initial Th disequilibrium, using an estimated Th/U ratio of 4 for the melt.
[e] Errors are 2σ; propagated using the algorithms of Ludwig [27].

University using the same analytical procedure as described in Spötl and Vennemann [37]. All measurements were done using a Thermo-Finnigan GasBench II equipped with a CTC Combi-Pal autosampler and linked to a Delta^{plus}XL mass spectrometer calibrated with Carrara Marble internal standard (2.05‰ C/−1.7‰ O) and NBS-19.

Reproducibility of replicate analyses was better than ±0.1‰ for standards and ±0.15‰ for sediment samples for both carbon and oxygen isotope ratios. All isotope results are reported in conventional δ notation defined as per mil (‰) deviation vs. VPDB.

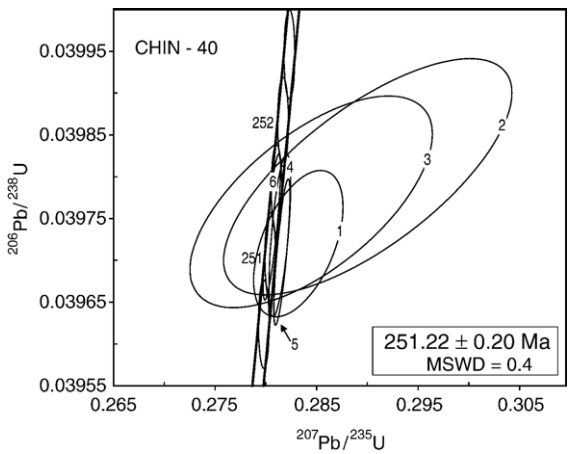

Fig. 3. Concordia plots showing the results of single-zircon analyses from the volcanic ash layer sample (CHIN-40) from the early Smithian "*Kashmirites densistriatus* beds". Individual analyses are shown as 2σ error ellipses. Numbers correspond to zircon numbers displayed in Table 1. The given age is a weighted mean $^{206}Pb/^{238}U$ age at 95% confidence level.

5.2. Results

All analytical data ($\delta^{13}C_{carb}$ and $\delta^{18}O_{carb}$) are provided in Supplementary Table 1 in the Appendix. In Fig. 2, the measured carbonate carbon isotope ratios are plotted against the composite profile. This profile combines 6 sections sampled in the vicinity of the villages of Jinya and Waili. The composite section has been compiled by means of lithological markers (i.e. sharp lithological changes, volcanic ash layers), which, as demonstrated by the refined ammonoid age control, are synchronous. The assessment of possible diagenetic overprints of the isotope record of the Jinya/Waili area is discussed in Galfetti et al. [6].

Beside the widely recognized Permian–Triassic boundary negative excursion, the C-isotope trend shows essentially 4 positive and 3 negative excursions between this boundary and the Early/Middle Triassic boundary.

The most significant negative excursion (from ca. 4.2‰ to −0.2‰) straddles the Permian–Triassic boundary. More positive values are detected within the late Griesbachian – early Dienerian interval. Stable values around 0.6‰ occur during most of the Dienerian. A second moderate positive excursion coincides with the onset of organic-rich shale deposition of early Smithian age ("*H. hedenstroemi* beds" and "*K. densistriatus* beds"). This excursion peaks just below the base of the "*F. rursiradiatus* beds" with values around 2.3‰ and is followed by a marked negative shift to values comprised between 1.5‰ and 0‰ at the base of the "*O. koeneni* beds". Although values from the "*O. koeneni* beds" are relatively scattered, they are comprised within a range between

−2‰ and 0‰. Such unusual low values (i.e. ∼−2‰) may be plausibly explained by an overprint of the carbon isotope record by deep burial diagenesis of the "*O. koeneni* beds" (see Galfetti et al. [6] for further details). A sharp and prominent positive shift (up to 4‰) coincides with organic-rich shale deposition of the latest Smithian "*A. multiformis* beds" (see also Galfetti et al. [6]). Peak C-isotope values of about 3‰ coincide with the onset of the nodular limestone at the very base of the Spathian ("Tirolitid n. gen. A beds"). Following this major C-isotope event, a gradual decrease to values of about −0.5‰ is observed within the middle part of the nodular limestone. A last positive excursion straddles the Spathian–Anisian boundary (i.e. "Transition beds") and differs remarkably from the previous ones by its gradual increase of the C-isotope values from the middle Spathian onward. The Anisian C-isotope trend shows a moderate decrease to values around 0‰.

5.2.1. Comparison with other Early Triassic carbon isotope records

Despite differences in depositional environments (i.e. facies and bathymetry), the new carbon isotope curve from the Early Triassic Luolou Fm. correlates well with other published carbon isotope records from the Tethyan and Boreal realms, confirming the global significance of the carbon isotope record within the Early Triassic (see [1,2,4–6,12,38] for review).

Our C-isotope data from the Jinya/Waili section reproduce the widely recognized negative excursion at the Permian–Triassic boundary (e.g. [39,10]). More positive $\delta^{13}C_{carb}$ values characterize the middle–late Griesbachian/early Dienerian interval. Similar trends with comparatively lower magnitudes, known from Dawen, Dajiang and Meishan (S-China [3,40]), Abadeh and Zal (Iran [4,41,38]) and are also recorded in the Jinya/Waili section.

The Dienerian–Smithian positive excursion, which has been outlined first at Losar (N-India [2]) and later at Dawen/Dajiang (S-China [3]), Wadi Wasit South (Oman [4]), Pufels, Uomo (Italy [41,42]), Taškent (Turkey [4]), Abadeh, Zal, Amol (Iran [38]), Muth (N-India; Richoz, personal communication, 2007) as well as at Chaohu and Pingdingshan (South China [43,40]), corresponds to the positive excursion occurring within the "*H. hedenstroemi* beds" and the "*K. densistriatus* beds" of the Luolou Fm. Whatever the final substage assignment of these ammonoid beds might be (see Section 4), the magnitude of this shift is much lower in the outer platform series of the Jinya/Waili area (+2.2‰) compared to the nearby (∼100 km) inner platform thrombolite-bearing cyclic limestone of the Great Bank of Guizhou (+8‰) [3]. Similarly high positive values (+6‰) are also documented from the calciturbidites at Wadi Wasit South (Oman [4]), from the shallow, subtidal siliciclastic–carbonate rocks at Uomo (Italy [42]), and from the shallow water, oolite-bearing limestones at Taškent (Turkey [4]), Abadeh, Zal and Amol (Iran [38]). Hence, it appears that this positive shift reaches much higher C-isotope ratios in inner platform settings, and/or in carbonate rocks directly transported by turbiditic currents from such shallow water settings. A general trend to higher C-isotope values in proximal depositional settings is known from Devonian [44], Triassic [40] and Cretaceous [45] examples. However, for the late Dienerian–early Smithian interval, differences of 4‰ to 6‰ between proximal and distal settings appear as extremes and are difficult to explain, especially when comparing the Dawen/Dajiang sections of the Great Bank of Guizhou [3] and the Jinya/Waili area, which both belong to the same basin and are located only ∼100 km far apart.

One of the most intriguing features of the Early Triassic carbon isotope record is the prominent late Smithian–early Spathian ("*A. multiformis* beds" – "Tirolitid n. gen. A beds") positive carbon isotope shift, which follows the typical low $\delta^{13}C_{carb}$ values of the middle Smithian ("*O. koeneni* beds"). The global extent of this shift has been demonstrated by its occurrence at Guandao, Chaohu, Majiashan, Pingdingshan (S-China [46,3,40]), Losar (N-India [2]), Nammal Gorge, Landu Nala (Pakistan [1,2]), Uomo (N-Italy [42]), Zal (Iran [38]), Sal (Oman [4]) and Dicksonfjellet (Spitsbergen [12]). Peak $\delta^{13}C_{carb}$ values usually reach ∼2‰, except for the Chaohu, Majiashan, Pingdingshan and Sal sections with values ranging from +4‰ to +8‰. This major excursion, coinciding with a global regressive–transgressive cycle [47–49] and organic-rich shale deposition in Jinya (South China [6]) and in Losar (North India [6]), is coupled (i) with the most drastic ammonoid/conodont turnover (i.e. extinction followed by radiation) ever detected within the entire Early Triassic [50,51], (ii) with a major change in spore–pollen assemblages in the Boreal Realm [52,12], and (iii) with the end of the radiolarite gap in the Tethys and in the low-latitude Panthalassa [53].

The well-expressed Spathian–Anisian positive carbon isotope shift, which follows low middle Spathian $\delta^{13}C_{carb}$ values, has already been identified at Losar (N-India [2]), Desli Caira (Romania [2]), Kçira (Albania [2]), Guandao (S-China [3]), Palazzo Adriano (Italy [41]) and at Jinya (S-China [6]). This protracted

excursion coincides with another major regressive–transgressive cycle [48] and with a moderate ammonoid/conodont turnover [54,51]. Maximal C-isotope values of this long-term perturbation locally range from +3‰ to +4.5‰, without clear trends related to bathymetry.

6. Implications for the calibration of the carbon isotope curve

As previously pointed out by Ovtcharova et al. [7], the calibration of Early Triassic ammonoid biochronozones

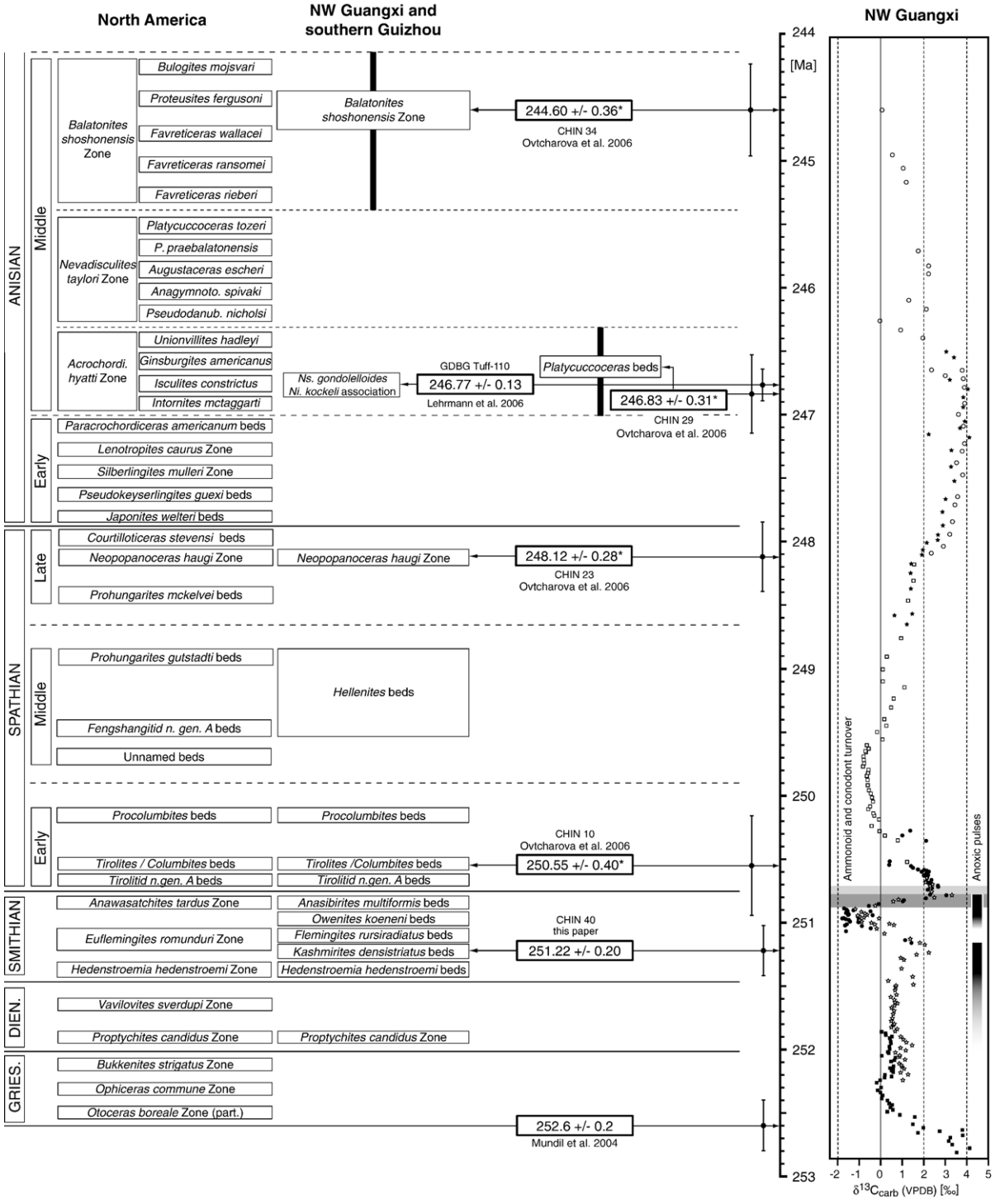

with U–Pb ages demonstrate that the four Early Triassic substages are of extremely uneven duration. The new early Smithian "*K. densistriatus* beds" U–Pb age allows narrowing down the duration of the Griesbachian–Dienerian interval as well as the duration of the Smithian substage, which are estimated to be ca. 1.4±0.4 My and to ca. 0.7±0.6 My, respectively. A minimal duration of 2.4±0.9 My has been inferred for the Spathian [7]. Recalculations of analytical uncertainties of the previously published Spathian U–Pb ages [7] now lead to a minimal duration of 2.4±0.7 My, thus confirming that it represents about half of the duration of the entire Early Triassic. The integration of these high-precision U–Pb ages with the new Early – early Middle Triassic C-isotope record from northwestern Guangxi allows constraining the duration of the strongly fluctuating carbon isotope signal in the wake of the end-Permian biotic crisis. This calibration shows a striking contraction in time of the C-isotope shifts for the Smithian time interval (compare Figs. 2 and 4). Hence, following the major negative shift straddling the Permian–Triassic boundary, the major perturbations of the global carbon cycle appear to be restricted to the early Smithian – early Spathian time interval of less than 1 My duration (Fig. 4). C-isotope values also vary with comparable magnitudes before and after this time interval, but at a much slower rate. The two episodes of black, organic-rich shales in NW Guangxi and in the northern Indian margin (i.e. Losar section, cf. Galfetti et al. [6]) coincide with positive shifts falling within the time interval characterized by rapid changes in C-isotope ratios. At least one of these positive shifts (i.e. the end-Smithian shift) concurs with a major ammonoid and conodont extinction (Fig. 4) and is immediately followed by a marked climatic change at the Smithian–Spathian boundary [32,52,6,12]. Any hypothesis of causal mechanisms triggering this array of Early Triassic biotic and abiotic changes needs to be compatible with the documented C-isotope fluctuation rates. Since the accuracy of carbon cycle models heavily relies on a high-resolution time framework (e.g. [55]), the new age data set provided in this paper should lead to the improvement of future Early Triassic carbon cycle simulations.

7. Conclusion

A new high-precision U–Pb age of 251.22±0.20 Ma associated with the early Smithian ammonoid fauna of the "*K. densistriatus* beds" has been measured from the Early Triassic Luolou Fm. (northwestern Guangxi, South China). This new age (i) reduces the absolute age gap comprised in the time interval between the P/T boundary and the early Spathian and (ii) provides a fundamental tie point for the timing of the Early Triassic biotic recovery. Taking into account the Permian–Triassic boundary age of 252.6±0.2 Ma [9], a maximal duration of ca. 1.4±0.4 My has been estimated for the Griesbachian–Dienerian interval and a duration of ca. 0.7±0.6 My has been calculated for the Smithian. Alternatively, a Permian–Triassic boundary age of 251.4±0.3 Ma [36] leads to an unrealistic short duration of 200±500 ky (!) for the Griesbachian–Dienerian interval. Hence, the Permian–Triassic boundary age of Mundil et al. [9] – rather than that of Bowring et al. [36] – shows greater consistency with our new set of Early Triassic ages and should be preferred in future studies.

The integration of this new early Smithian U–Pb age with the ammonoid zonation and with recalculated uncertainties of previous Early/Middle Triassic ages [7] lead to the first precise calibration of the new high-resolution carbonate carbon isotope record ($\delta^{13}C_{carb}$) obtained from Early Triassic outer platform series (Luolou Fm.) of the Nanpanjiang Basin. The calibration of this C-isotope record and its correlation with other Early Triassic C-isotope curves demonstrates that the largest and fastest C-isotope perturbations take place essentially during the early Smithian – early Spathian time interval, a time span corresponding to less than 1 My.

The middle Smithian (i.e. "*F. rursiradiatus* beds") appears as the first major and global diversification episode for nektonic clades, such as ammonoids [56] and conodonts [51] characterized by intrinsic high evolutionary rates. The low diversity phases of these two clades coincide with the two major positive C-isotope excursions: (i) during the early Smithian and (ii)

Fig. 4. Calibration of carbonate carbon isotope data from northwestern Guangxi with ammonoid biochronozones and U–Pb ages. The recalculated analytical uncertainties of previously published U–Pb ages [7] are marked with an asterisk (*) (see Section 3 for further details). Uncertainties in the biochronological correlations between the high-resolution North American ammonoid zonation and the South Chinese paleontological ages are indicated by thick vertical black bars. Ammonoid data are compiled from the following sources: Griesbachian and Dienerian from North America [35]; Spathian from North America [16,17] and Bucher et al. (ongoing work). Anisian from North America [67,68]; Smithian from NW Guangxi (Brayard and Bucher [56]); Spathian from NW Guangxi (Bucher et al., ongoing work). Among the four U–Pb ages reported from S-Guizhou by Lehrmann et al. [8], only one tuff (GDGB – Tuff 110) is associated with conodonts allowing unequivocal and precise correlation with the North American ammonoid faunas (i.e. the *Isculites constrictus* subzone). Note the anoxic trends (darker shading denotes greater intensity of anoxia) and the ammonoid/conodont turnover (i.e. extinction [dark grey] followed by a radiation [light grey]) around the Smithian–Spathian boundary. Abbreviations: Gries = Griesbachian; Dien = Dienerian.

during the latest Smithian. As shown by ammonoid taxonomic diversity and paleobiogeographic distribution patterns, high diversity values are concomitant with the resumption of the biogeographical differentiation, essentially manifested by steep latitudinal diversity gradients [32]. On the other hand, benthic clades with comparatively low evolutionary rates (e.g. ostracods [57], gastropods [58]) did not start recovering until Spathian time, i.e. when the rates of the C-isotope fluctuations slowed down. Moreover, recently it has been shown that the major ammonoid and conodont evolutionary turnover concur with climatic changes as inferred from boreal palynological assemblages and with the global positive C-isotope excursion recorded around the Smithian–Spathian boundary [12].

What cause(s) led to these profound Early Triassic biotic and abiotic changes remain speculative, especially in the absence of a complete and high-resolution organic carbon isotope record. The global, latest Smithian, positive C-isotope perturbation reflected in the inorganic [2,3,4,40,6] and organic carbon reservoirs [12] could be eventually explained by an enhanced storage and preservation of organic matter in the ocean. To date, the best evidence for Early Triassic black shales comes from the deep-sea Panthalassic record (e.g. Japan [59]). This increased storage may be explained by anoxia and/or by an increase in primary production (e.g. [60]). By analogy with analogous carbon cycle perturbations in the Devonian [61], Jurassic [62], Cretaceous [63], and according to a recently published Early Triassic carbon cycle model [55], phases of CO_2 degassing via volcanism appear as a conceivable trigger for global carbon cycle disturbance. In such a scenario, a sustained phase of repeated CO_2 injections might occur during middle Smithian times ("*F. rursiradiatus* and *O. koeneni* beds"), for which the most significant and fastest negative shift from +2‰ to ca. −1‰ is documented. The steep, positive C-isotope shift around the Smithian–Spathian boundary could therefore represent the biosphere response to altered pCO_2 levels.

As already pointed out [7,6,12], the protracted magmatic activity in the Siberian Basin (e.g. [64]) makes this area a likely volcanic source for a massive CO_2 supply during the Early Triassic. Additionally, the metabasic lavas of supposedly Early to Middle Triassic age of the Nilüfer Unit (N-Turkey [65,66]), which have also been interpreted as remnants of a large igneous province, could be considered as a potential and supplementary CO_2 source. The short duration of the P/T boundary – early Spathian interval (2.0±0.6 My) makes a causal connection between the documented C-isotope perturbations and the volcanic activity quite probable. However, direct evidence for such volcanic activity during the Smithian is still missing. On the other hand, none of the presently available data from the Siberian Basin permit to exclude an additional eruptive phase some 1.5 to 2 My after the main eruptive activity.

Acknowledgements

S. Bruchez and T. Vennemann are thanked for measuring carbon and oxygen isotopes at the Institute of Mineralogy and Geochemistry (Lausanne University). M. Orchard shared useful information on conodont–ammonoid intercalibration of the North American ammonoid succession. T.G. is grateful to L. Pauli and J. Huber for lab assistance. We wish to thank two anonymous reviewers for constructive criticisms during the review process. U–Pb analyses were supported by the Swiss NSF project 200021-103335 (to U.S.). This research was supported by the Swiss NSF project 200020-113554 (to H. Bucher). Contribution Nr. UMR5125-07.016 (A. Brayard, F. Cordey).

Appendix A. Supplementary data

Supplementary data associated with this article can be found, in the online version, at doi:10.1016/j.epsl.2007.04.023.

References

[1] A. Baud, V. Atudorei, Z. Sharp, Late Permian and Early Triassic evolution of the Northern Indian margin: carbon isotope and sequence stratigraphy, Geodinamica Acta 9 (1996) 57–77.
[2] V. Atudorei, Constraints on the Upper Permian to Upper Triassic marine carbon isotope curve. Case studies from the Tethys. Ph.D. thesis, University of Lausanne, Switzerland, 1999.
[3] J.L. Payne, D.J. Lehrmann, J. Wei, M.J. Orchard, D.P. Schrag, A.H. Knoll, Large perturbations of the carbon cycle during recovery from the end-Permian extinction, Science 305 (2004) 506–509.
[4] S. Richoz, Stratigraphie et variations isotopiques du carbone dans le Permien supérieur et le Trias inférieur de la Néotéthys (Turquie, Oman et Iran). Ph.D. thesis, University of Lausanne, Switzerland, 2004.
[5] F.A. Corsetti, A. Baud, P.J. Marenco, S. Richoz, Summary of Early Triassic carbon isotope records, Comptes Rendus Palevol 4 (2005) 405–418.
[6] T. Galfetti, H. Bucher, A. Brayard, P.A. Hochuli, H. Weissert, K. Guodun, V. Atudorei, J. Guex, Late Early Triassic climate change: insights from carbonate carbon isotopes, sedimentary evolution and ammonoid paleobiogeography, Palaeogeography Palaeoclimatology Palaeoecology 243 (2007) 394–411.
[7] M. Ovtcharova, H. Bucher, U. Schaltegger, T. Galfetti, A. Brayard, J. Guex, New Early to Middle Triassic U–Pb ages from South China: calibration with ammonoid biochronozones and implications for the timing of the Triassic biotic recovery, Earth Planetary Science Letters 243 (2006) 463–475.

[8] D.J. Lehrmann, J. Ramezani, S.A. Bowring, M.W. Martin, P. Montgomery, P. Enos, J.L. Payne, M.J. Orchard, W. Hongmei, W. Jiayong, Timing of recovery from the end-Permian extinction: geochronologic and biostratigraphic constraints from south China, Geology 34 (2006) 1053–1056.
[9] R. Mundil, K.R. Ludwig, I. Metcalfe, P.R. Renne, Age and timing of the Permian mass extinctions: U/Pb dating of closed-system zircons, Science 305 (2004) 1760–1763.
[10] A. Baud, M. Magaritz, W.T. Holser, Permian–Triassic of the Tethys: carbon isotope studies, Geologische Rundschau 78 (1989) 649–677.
[11] J.S. Chen, X.L. Chu, M.R. Shao, H. Zhong, Carbon isotope study of the Permian Triassic boundary sequences in China, Chemical Geology 86 (1991) 239–251.
[12] T. Galfetti, P.A. Hochuli, A. Brayard, H. Bucher, H. Weissert, J.O. Vigran, Smithian/Spathian boundary event: evidence for global climatic change in the wake of the end-Permian biotic crisis, Geology 35 (2007) 291–294.
[13] D.J. Lehrmann, J.Y. Wei, P. Enos, Controls on facies architecture of a large Triassic carbonate platform: The Great Bank of Guizhou, Nanpanjiang Basin, South China, Journal of Sedimentary Research 68 (1998) 311–326.
[14] S. Kershaw, L. Guo, A. Swift, J.S. Fan, Microbialites in the Permian–Triassic boundary interval in Central China: structure, age and distribution, Facies 47 (2002) 83–89.
[15] S. Crasquin-Soleau, J. Marcoux, L. Angiolini, A. Nicora, Palaeocopida (Ostracoda) across the Permian–Triassic events: new data from South-Western Taurus (Turkey), Journal of Micropalaeontology 23 (2004) 67–76.
[16] J. Guex, A. Hungerbühler, J. Jenks, D. Taylor, H. Bucher, Dix-huit nouveaux genres d'ammonites du Spathien (Trias inférieur) de l'Ouest américan (Idaho, Nevada, Californie): note préliminaire, Bullettin de Géologie Lausanne 362 (2005) 1–31.
[17] J. Guex, A. Hungerbühler, J. Jenks, D. Taylor, H. Bucher, Dix-neuf nouvelles espèces d'ammonites du Spathien (Trias inférieur) de l'Ouest américan (Idaho, Nevada, Californie): note préliminaire, Bulletin de Géolgie Lausanne 363 (2005) 1–25.
[18] N. Hori, Triassic radiolarians from chert of the Chichibu Belt in the Toyohashi district, Aichi Prefecture, Southwest Japan, Bulletin of the Geological Survey Japan 55 (2004) 303–334.
[19] K. Sugiyama, Triassic and Lower Jurassic radiolarian biostratigraphy in the siliceous claystone and bedded chert units of the southeastern Mino Terrane, central Japan, Bulletin Mizunami Fossil Museum 24 (1997) 79–193.
[20] R. Mundil, I. Metcalfe, K.R. Ludwig, P.R. Renne, F. Oberli, R.S. Nicoll, Timing of the Permian–Triassic biotic crisis: implications from new zircon U/Pb age data (and their limitations), Earth and Planetary Science Letters 187 (2001) 131–145.
[21] D. Condon, M. Zhu, S. Bowring, W. Wang, A. Yang, Y. Jin, U–Pb ages from the Neoproterozoic Doushantuo Formation, China, Science 308 (2005) 95–98.
[22] D.J. Cherniak, E.B. Watson, Pb diffusion in zircon, Chemical Geology 172 (2001) 5–24.
[23] J.M. Mattinson, Zircon U–Pb chemical abrasion ("CA-TIMS") method: combined annealing and multi-step partial dissolution analysis for improved precision and accuracy of zircon ages, Chemical Geology 200 (2005) 47–66.
[24] S.A. Bowring, M.D. Schmitz, High-precision U–Pb zircon geochronology and the stratigraphic record, Reviews in Mineralogy Geochemistry 53 (2003) 305–326.
[25] B. Schoene, S.A. Bowring, U–Pb systematics of the McClure Mountain syenite: thermochronological constraints on the age of the $^{40}Ar/^{39}Ar$ standard MMhb, Contributions to Mineralogy and Petrology 151 (2006) 615–630.
[26] B. Schoene, J.L. Crowley, D.C. Condon, M.D. Schmitz, S.A. Bowring, Reassessing the uranium decay constants for geochronology using ID-TIMS U–Pb data, Geochimica et Cosmochimica Acta 70 (2006) 426–445.
[27] K.R. Ludwig, Calculations of uncertainties of U–Pb isotope data, Earth Planetary Science Letters 46 (1980) 212–220.
[28] D.J. Lehrmann, P. Enos, J.L. Payne, P. Montgomery, J. Wei, Y. Yu, J. Xiao, M.J. Orchard, Permian and Triassic depositional history of the Yangtze platform and Great Bank of Guizhou in the Nanpanjiang Basin of Guizhou and Guangxi, South China, Albertiana 33 (2005) 149–168.
[29] K. Ludwig, Isoplot/Ex.V.3. USGS Open-File repository, 2005.
[30] J.G. Ogg, The Triassic period, in: F.M. Gradstein, J.G. Ogg, A.G. Smith, (Eds.), A Geological Time Scale. Cambridge Univ. Press, 2004, pp. 271–306.
[31] G. Escarguel, H. Bucher, Counting taxonomic richness from discrete biochronozones of unknown duration: a simulation, Palaeogeography Palaeoclimatology Palaeoecology 202 (2004) 181–208.
[32] A. Brayard, H. Bucher, G. Escarguel, F. Fluteau, S. Bourquin, T. Galfetti, The Early Triassic ammonoid recovery: paleoclimatic significance of diversity gradients, Palaeogeography Palaeoclimatology Palaeoecology 239 (2006) 374–395.
[33] J. Guex, Biochronologic Correlations. Springer-Verlag, 1991.
[34] A.S. Dagys, Lower Triassic stage, substage and zonal scheme of north-eastern Asia, Mémoires Géollogie (Lausanne) 22 (1994) 15–23.
[35] E.T. Tozer, Canadian Triassic ammonoid faunas, Geological Survey of Canada Bulletin 467 (1994) (663 pp.).
[36] S.A. Bowring, D.H. Erwin, Y.G. Jin, M.W. Martin, K. Davidek, W. Wang, U/Pb zircon geochronology and tempo of the end-Permian mass extinction, Science 280 (1998) 1039–1045.
[37] C. Spötl, T.W. Vennemann, Continuous-flow isotope ratio mass spectrometric analysis of carbonate minerals, Rapid Communications Mass Spectrometry 17 (2003) 1004–1006.
[38] M. Horacek, S. Richoz, R. Brandner, L. Krystyn, C., Spötl, Evidence for recurrent changes in Lower Triassic oceanic circulation of the Tethys: the $\delta^{13}C$ record from marine sections in Iran, Palaeogeography Palaeoclimatology Palaeoecology (in press), doi:10.1016/j.palaeo.2006.11.052.
[39] W.T. Holser, M. Magaritz, Events near the Permian–Triassic boundary, Modern Geology 11 (1987) 155–180.
[40] J. Zuo, J. Tong, H. Qiu, L. Zhao, Carbon isotope composition of the Lower Triassic marine carbonates, Lower Yangtze Region, South China, Science in China Series D: Earth Sciences 49 (2006) 225–241.
[41] C. Korte, H.W. Kozur, J. Veizer, $\delta^{13}C$ and $\delta^{18}O$ values of Triassic brachiopods and carbonate rocks as proxies for coeval seawater and palaeotemperature, Palaeogeography Palaeoclimatology Palaeoecology 226 (2005) 287–306.
[42] M. Horacek, R. Brandner, R. Abart, Carbon isotope record of the P/T boundary and the Lower Triassic in the Southern Alps: evidence for rapid changes in storage of organic carbon, Palaeogeography Palaeoclimatology Palaeoecology (in press), doi:10.1016/j.palaeo.2006.11.049.
[43] J. Tong, D.H. Erwin, Z. Jingxun, Z. Laishi, Lower Triassic carbon isotope stratigraphy in Chaohu, Anhui: implication to biotic and ecological recovery, Albertiana 33 (2005) 75–76.

[44] W. Buggisch, M.M. Joachimski, Carbon isotope stratigraphy of the Devonian of Central and Southern Europe, Palaeogeography Palaeoclimatology Palaeoecology 240 (2006) 68–88.
[45] H.C. Jenkyns, Carbon-isotope stratigraphy and paleoceanographic significance of the Lower Cretaceous shallow-water carbonates of Resolution Guyot, mid-Pacific Mountains, in: E.L. Winterer, W.W. Sager, J.V. Firth, J.M. Sinton (Eds.), Proceedings of the Ocean Drilling Program, Scientific Results, 143, 1995, pp. 99–104.
[46] J. Tong, Y.D. Zakharov, M.J. Orchard, Y. Hongfu, H.J. Hansen, A candidate of the Induan–Olenekian boundary stratotype in the Tethyan region, Science in China Series D 46 (2003) 1182–1200.
[47] R.A. Paull, R.K. Paull, Interpretation of Early Triassic nonmarine–marine relations, Utah, USA, in: S.G. Lucas, M. Morales (Eds.), The Nonmarine Triassic, New Mexico Museum of Natural History and Science Bulletin, 1993.
[48] A.F. Embry, Global sequence boundaries of the Triassic and their identification in the Western Canada sedimentary basin, Bulletin of Canadian Petroleum Geology 45 (1997) 415–433.
[49] J. Tong, H. Yin, K. Zhang, Permian and Triassic sequence stratigraphy and sea level changes of eastern Yangtze platform, Journal of China University of Geosciences 10 (1999) 161–169.
[50] E.T. Tozer, Marine Triassic faunas of North America: their significance for assessing plate and terrane movements, Geologische Rundschau 71 (1982) 1077–1104.
[51] M.J. Orchard, Conodont diversity and evolution through the latest Permian and Early Triassic upheavals, Palaeogeography Palaeoclimatology Palaeoecology (in press), doi:10.1016/j.palaeo.2006.11.037.
[52] P.A. Hochuli, T. Galfetti, A. Brayard, H. Bucher, J.O. Vigran, H. Weissert, The major climatic turnover of the late Early Triassic: the Smithian/Spathian boundary event, in: H.A. Nakrem, A. Mørk (Eds.), Boreal Triassic, Geological Society of Norway, Longyearbyen, Svalbard, 2006, p. 59.
[53] H.W. Kozur, Some aspects of the Permian–Triassic boundary (PTB) and of the possible causes for the biotic crisis around this boundary, Palaeogeography Palaeoclimatology Palaeoecology 143 (1998) 227–272.
[54] H. Bucher, Lower Anisian ammonoids from the northern Humboldt Range (northwestern Nevada, USA) and their bearing upon the Lower–Middle Triassic boundary, Eclogae Geologicae Helvetiae 82 (1989) 943–1002.
[55] J.L. Payne, L.R. Kump, Evidence for recurrent Early Triassic massive volcanism from quantitative interpretation of carbon isotope fluctuations, Earth Planetary Science Letters 256 (2007) 264–277.
[56] A. Brayard, H. Bucher, Smithian (Early Triassic) ammonoid faunas from northwestern Guangxi (South China): Taxonomy and Biochronology. Fossils and strata, submitted for publication.
[57] S. Crasquin-Soleau, T. Galfetti, H. Bucher, A. Brayard, Palaeoecological changes after the end-Permian mass extinction: Early Triassic ostracods from northwestern Guangxi Province, South China, Rivista Italiana di Paleontologia e Stratigrafia 112 (2006) 55–75.
[58] J.L. Payne, Evolutionary dynamics of gastropod size across the end-Permian extinction and through the Triassic recovery interval, Paleobiology 31 (2005) 269–290.
[59] N. Suzuki, K. Ishida, Y. Shinomiya, H. Ishiga, High productivity in the earliest Triassic ocean: black shales, Southwest Japan, Palaeogeography Palaeoclimatology Palaeoecology 141 (1998) 53–65.
[60] A.P. Menegatti, H. Weissert, R.S. Brown, R.V. Tyson, P. Farrimond, A. Strasser, M. Caron, High-resolution delta C-13 stratigraphy through the early Aptian "Livello Selli" of the Alpine Tethys, Paleoceanography 13 (1998) 530–545.
[61] D. Chen, H. Qing, R. Li, The Late Devonian Frasnian–Famennian (F/F) biotic crisis: Insights from $\delta^{13}C_{carb}$, $\delta^{13}C_{org}$ and $^{87}Sr/^{86}Sr$ isotopic systematics, Earth Planetary Science Letters 235 (2005) 151–166.
[62] H.C. Jenkyns, C.J. Clayton, Black shales and carbon isotopes in pelagic sediments from the Tethyan Lower Jurassic, Sedimentology 33 (1986) 87–106.
[63] H. Weissert, E. Erba, Volcanism, CO_2 and palaeoclimate: a Late Jurassic–Early Cretaceous carbon and oxygen isotope record, Journal of the Geological Socciety 161 (2004) 695–702.
[64] A.V. Ivanov, S.V. Rasskazov, G.D. Feoktistov, H. He, A. Boven, $^{40}Ar/^{39}Ar$ dating of Usol'skii sill in the south-eastern Siberian Traps Large Igneous Province: evidence for long-lived magmatism, Terra Nova 17 (2005) 203–208.
[65] O. Kaya, H. Mostler, A Middle Triassic Age for low-grade greenschist facies metamorphic sequence in Bergama (Izmir), Western Turkey – the 1st Paleontological Age Assignment and Structural–Stratigraphic Implications, Newsletters on Stratigraphy 26 (1992) 1–17.
[66] S. Can Genç, A Triassic large igneous province in the Pontides, northern Turkey: geochemical data for its tectonic setting, Journal of Asian Earth Sciences 22 (2004) 503–516.
[67] C. Monnet, H. Bucher, New Middle and Late Anisian (Middle Triassic) ammonoid faunas from northwestern Nevada: taxo- nomy and biochronology, Fossil and Strata 52 (2005) 121.
[68] C. Monnet, H. Bucher, Anisian (Middle Triassic) ammonoids from North America: quantitative biochronology and biodiversity, Stratigraphy 2 (2005) 281–296.